DOI 10.1007/s11141-021-10114-7
Radiophysics and Quantum Electronics, Vol. 64, No. 2, July, 2021
(Russian Original Vol. 64, No. 2, February, 2021)

DEVELOPMENT OF A METHOD FOR DETERMINING THE POSITION OF ARTIFICIAL IONOSPHERIC IRREGULIARITIES RESPONSIBLE FOR THE RADIO-WAVE ASPECT-ANGLE SCATTERING ON SHORT PATHS BY OBLIQUE BACKSCATTER SOUNDING IONOGRAMS

N. A. Pogorelko,[1*] **E. N. Sergeev,**[1] **S. M. Grach,**[1] **and E. Yu. Zykov** [2]

UDC 533.951+621.371

The data of experiments on the oblique backscatter sounding of the heated ionospheric volume above the Sura facility on a short Kazan — Vasilsursk — Kazan path, when the Cyclone-GPS ionosonde was operated in the ionogram recording regime in the frequency range 1–7 MHz with a step of about 20 kHz are compared with the results of ray-tracing calculations for the sounding and scattered signals of the O- and X-mode polarizations over the entire range of operating frequencies of the ionosonde. The dependences of the typical transverse (to the geomagnetic field) scales of artificial scattering irregularities (in the range 40–200 m), which are responsible for the aspect-angle scattering of radio waves of this range, and the position of the scattering region on the frequency of the sounding signals are determined for the entire range of existence of oblique backscatter sounding ionograms.

1. INTRODUCTION

Electron-density irregularities aligned with the geomagnetic field $\mathbf{B}$ and having transverse scales from a few centimeters to hundreds of meters are generated in the region of reflection of high-power HF radio waves as they affect the Earth's ionosphere [1–7]. When the Bragg conditions

$$\mathbf{k}_\mathrm{d} = \mathbf{k}_\mathrm{s} \pm \boldsymbol{\kappa} \tag{1}$$

are fulfilled, these irregularities cause aspect-angle scattering, including backscatter, of radio waves propagating through the heated ionospheric volume. Here, $\mathbf{k}_\mathrm{d}$ and $\mathbf{k}_\mathrm{s}$ are the wave vectors of the incident (diagnostic) and scattered waves, respectively, $k_\mathrm{d} \approx k_\mathrm{s} = 2\pi f n/c$, f and n are the frequencies and the modulus of the refractive index of the incident and scattered waves, c is the speed of light, and $\boldsymbol{\kappa}$ is the wave vector of the electron-density irregularity, $\boldsymbol{\kappa} \perp \mathbf{B}$. In the case of backscattering ($\mathbf{k}_\mathrm{d} = -\mathbf{k}_\mathrm{s}$), $\kappa = 2k_\mathrm{d}$. Thus, by measuring the characteristics of aspect-angle scattering, it is possible to analyze the spatial spectrum of artificial irregularities and their location in the heated ionospheric volume.

A large amount of data on studies of the heated ionospheric volume using aspect-angle scattering was accumulated for HF sounding wave in the frequency range 7–30 MHz [8–10]. The lengths of the sounding/scattered signal paths in such experiments exceed several hundred kilometers, and the frequencies of scattered signals at the point of their reception are usually higher than the critical frequencies of the F layer. A detailed algorithm for spatial positioning of the scattering region and determining its spatial structure

* pogorelko_n_a@mail.ru

[1] N. I. Lobachevsky State University of Nizhny Novgorod, Nizhny Novgorod; [2] Kazan Federal University, Kazan, Russia. Translated from Izvestiya Vysshikh Uchebnykh Zavedenii, Radiofizika, Vol. 64, No. 2, pp. 95–108, February 2021. Russian DOI: 10.52452/00213462_2021_64_02_95 Original article submitted August 8, 2020; accepted November 24, 2020.

is described in [8–10]. The algorithm used ray-tracing calculations in a nonuniform magnetized ionosphere with allowance for the measured delays and angles of arrival of the scattered signal in the horizontal and vertical planes.

The study of the propagation and scattering of HF radio waves in the Earth's ionosphere disturbed by high-power radio emission at frequencies near and below the critical frequencies of the F_2 layer is an independent applied problem of propagation of electromagnetic waves in a magnetized plasma. The first experimental studies on the aspect-angle scattering of waves of this frequency range by artificial plasma-density irregularities that are strongly elongated along the geomagnetic field and have transverse dimensions of the order of the sounding radio wave length were conducted at the Zimyonki (Gorky) and Tromsø (Norway) facilities [11, 12]. The Bragg backscattering condition for such radio waves, when the sounding transmitter and the receiver of scattered waves are located in one place, is well fulfilled on short radio paths due to strong refraction. In this case, the ionospheric conditions along the path can be considered approximately constant. In addition, the impact of the geomagnetic field on the propagation of radio waves is more significant in this frequency range, which complicates the calculations. Such experiments make it possible not only to study the propagation trajectories of radio signals, but also to explore the location of artificial ionospheric irregularities responsible for scattering of the radio signals and their characteristics.

In [13], the data of the experiments on aspect-angle backscattering at frequencies of 2–7 MHz performed on a short Kazan — Vasilsursk — Kazan path using the Sura facility (Vasilsursk) [14] are compared with the results of ray-tracing calculations for the sounding and scattered signals, the position of the region above the Sura facility responsible for the generation of aspect-angle scattering signals is determined, and the typical scales of scattering irregularities are found.

The Cyclone-GPS ionosonde of Kazan Federal University, located 172 km east of the Sura facility, which emitted sounding signals and detected scattered signals at 10 fixed frequencies, was used in the experiments [14]. A family of scattered rays coming into the reception area was determined for the calculated trajectories in accordance with the Bragg condition. Herein, the calculated propagation time of the oblique backscatter sounding signal should coincide with the experimentally observed delay time. As a result, the position and sizes of the regions above the Sura facility that are responsible for the generation of aspect-angle scattering signals of different frequencies, the typical scales of artificial scattering irregularities, and their dynamic characteristics as functions of the generation altitude and the time of the day were determined.

The choice of the sounding frequencies of the ionosonde was performed in the frequency range where the scattered signal was observed and was determined by the technical characteristics of the radiation transmitter and the necessary time resolution of the measurements (approximately 0.5 s). The interval between adjacent frequencies was 300–600 kHz. A grid of 256 frequencies of sounding waves with a step of about 20 kHz is used for routine operation of the ionosonde in the ionogram recording mode. In this case, along with the vertical sounding ionograms, the oblique backscatter sounding ionograms related to scattering of the sounding signals by irregularities in the heated volume above the Sura facility are recorded during a long (stationary) heating of the ionosphere. The objective of this paper is to study the characteristics of the heated volume with such oblique backscatter sounding ionograms using the same calculation algorithm as in [13]. The frequency grid used for taking ionograms provides the determination of an almost continuous dependence of the position of the scattering region on the frequency of the sounding signal. This improves the method of finding the position of scattering artificial ionospheric irregularities in the heated volume and their typical scales.

2. EXPERIMENT SETTING UP AND MEASUREMENT RESULTS

Data of the experiments conducted on September 20 and 24, 2010 were used to analyze the characteristics of the heated volume, namely, on September 24 with a vertical impact on the ionosphere and on September 20 with the radiation pattern tilted by 12° southward from the vertical line in the magnetic meridian plane. The Sura facility was continuously operated at $f_0 = 4.74$ MHz from 16:50 to 21:40 MSK in the 20-min radiation — 10-min pause regime. The effective radiation power of the facility was 60 MW

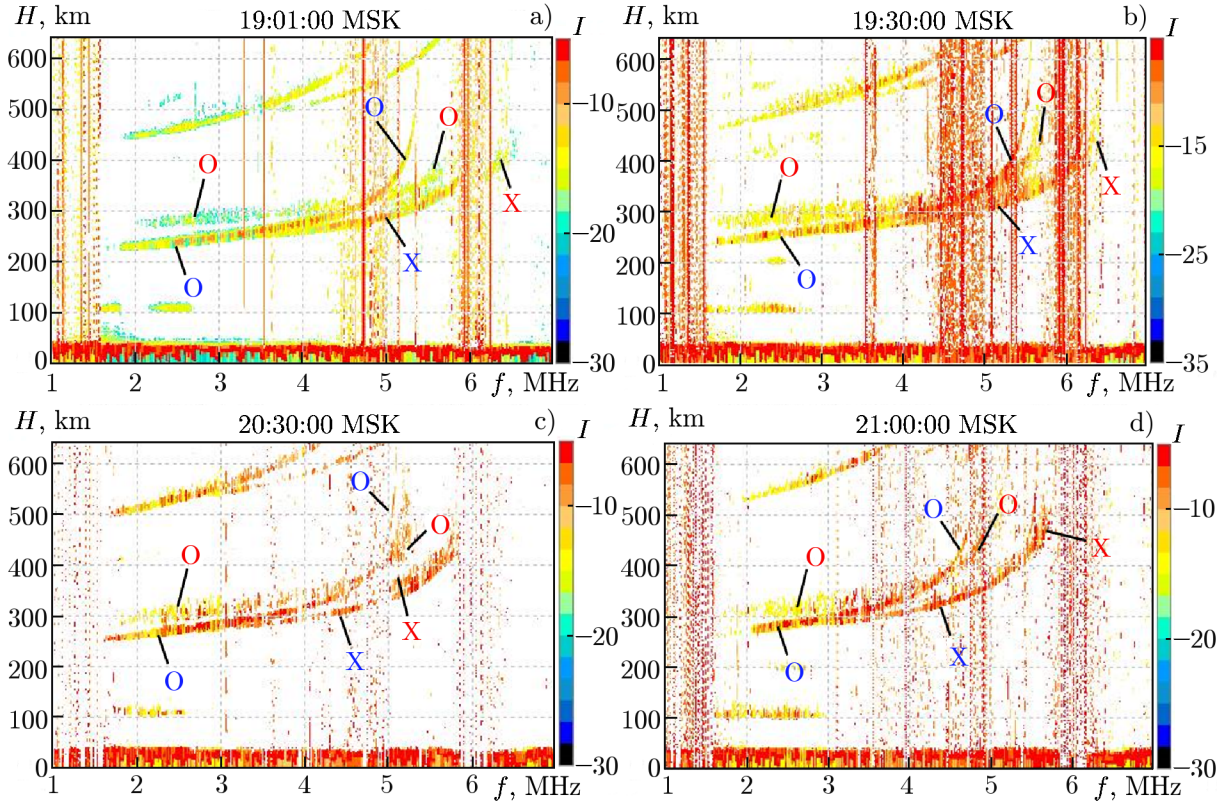

Fig. 1. Experiment on vertical heating of the ionosphere above the Sura facility on September 24, 2010: the ionograms recorded by Cyclone-GPS. The ordinary and extraordinary modes are denoted O and X, respectively. The blue font corresponds to vertical sounding and the red font, to oblique backscatter sounding. The signal intensity I (as in Figs. 2, 3, and 6) is given in ionosonde ADC units.

(two transmitters were used on September 24) and 120 MW (three transmitters of the heater were used on September 20). The Cyclone-GPS ionosonde was operated in the ionogram recording regime: it ran over 256 frequencies of sounding waves in the range from 1 to 7 MHz for 20 s in the middle of the heating session. This method made it possible to study the process of aspect-angle scattering of radio waves over the entire range of sounding frequencies.

Examples of the ionograms recorded on September 24, 2010 are given in Fig. 1. It shows vertical sounding ionograms (the ordinary and extraordinary components are marked in blue as O and X, respectively) and oblique backscatter sounding ionograms as traces corresponding to the ordinary and extraordinary components of aspect-angle scattered waves (marked in red).

Figure 2 shows examples of the ionograms recorded on September 20, 2010 for the case of oblique impact on the ionosphere at an angle of 12° to the south in the geomagnetic meridian plane (for the Sura facility, the tilt of the geomagnetic field to the vertical line (the magnetic zenith direction) in 2010 was 18.5° southward). In that experiment, as is seen in Fig. 2, there was dynamic variation of the scattered signal as a function of time: a decrease in the observed minimum scattering frequency from 3.5 to 2 MHz was observed between 17:30 and 19:00 MSK. However, this frequency has never fallen below the critical frequency of the E layer. The maximum observed frequencies (MOF) of scattering for both radiation modes could exceed the critical frequencies $f_{\mathrm{O}F_2}$ and $f_{\mathrm{X}F_2}$ of the F_2 layer by 0.3–0.7 MHz.

3. CALCULATION RESULTS FOR VERTICAL HEATING

The purpose of the calculations was to determine the parameters of the region responsible for the aspect-angle scattering (altitude and horizontal coordinates of the region projected on the Earth's surface)

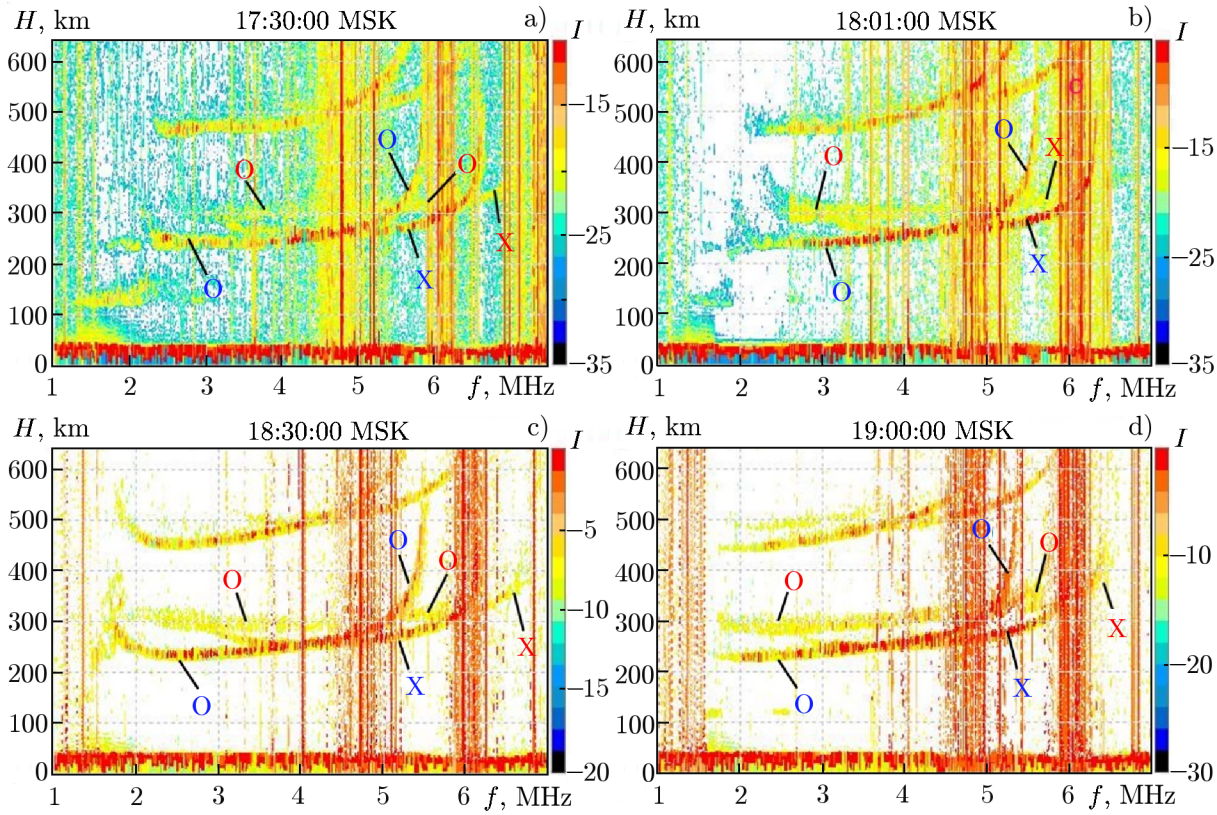

Fig. 2. Experiment on oblique heating of the ionosphere (the radiation pattern is tilted by 12° southward in the geomagnetic meridian plane) on September 20, 2010: the ionograms recorded by the Cyclone-GPS ionosonde. The ordinary and extraordinary modes are denoted O and X, respectively. The blue font corresponds to vertical sounding and the red font, to oblique backscatter sounding.

located within the HF-heated ionospheric region filled with field-aligned small-scale irregularities. The horizontal size of the heated volume is determined by its radius $R = h_c \tan(\beta/2)$, where $\beta = 12°$ is the half-power beamwidth for three operating antenna sections of the Sura facility ($\beta = 18°$ along the north–south line (NS) when two sections of the Sura antenna (two instead of three transmitters) operated at $f_0 = 4740$ kHz are used, and h_c is the altitude of the center of the horizontal cross section of the Sura radiation pattern in the scattering region. The trajectories of the sounding and scattered signals were calculated in the ray-tracing approximation within the framework of the model of a spherically layered, magnetized ionospheric plasma [15] for a family of rays filling the cone at the radiation point and the central ray oriented in the Kazan direction — the expected position of the scattering region (where the Bragg condition is fulfilled) above the Sura facility (Vasilsursk) and an 1° opening. The angle α of incidence of the central ray on the ionosphere varied in the range of 25°–50°. The angle of deflection of the central ray from the north to the west projected on the horizontal plane in the calculations varied within $\varphi = 77°$–$85°$ for the vertical impact ($\varphi = 80.5°$ corresponds to radiation of a diagnostic wave across the geomagnetic meridian plane) and within $\varphi = 76°$–$96°$ with the Sura radiation pattern tilted southward. Eastern declination of the magnetic field 10.7° and an inclination of 71.6° were specified in the calculations in accordance with the IGRF geomagnetic field model [16].

When the probing ray falls into the scattering region, a family of scattered beams arriving at the signal reception zone near the Cyclone ionosonde, which approximately corresponds to the first several Fresnel zones at respective frequency [13, 17, 18], were determined in accordance with the Bragg condition. Herein, the calculated time of propagation of the signal along the oblique backscatter sounding path should coincide with the experimentally observed delay time $\tau = H/c \approx 0.8$–1.8 ms (H is the effective altitude, or is the range for

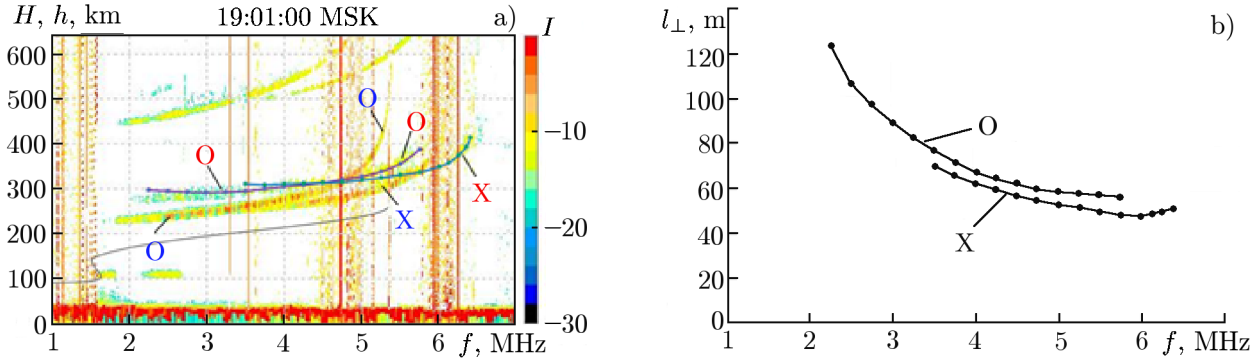

Fig. 3. Panel *a*: ionograms of vertical (marked in blue) and oblique backscatter (marked in red) sounding during vertical heating of the ionosphere (September 24, 2010, Cyclone-GPS ionosonde), calculated curves of the scattered-signal delay times in units of the effective altitude H (black and green solid curves with markers), and the dependence of the true reflection altitudes h on the frequency according to vertical sounding data (solid curve). Panel *b*: dependence of the transverse scale $l_\perp$ of the scattering irregularity on the sounding frequency.

oblique sounding, and c is the speed of light; see Figs. 1 and 2). More precisely, the calculated time should fall into the scatter interval $\Delta\tau \approx 50$–100 μs determined by the width of the trace of the oblique backscatter sounding ionogram in Figs. 1 and 2. Note that for the experiment geometry, when the ionosphere is vertically affected, the angle γ between the geomagnetic field $\mathbf{B}$ and the wave vector $\mathbf{k}_\mathrm{d}$ of the probing rays coming into the scattering region is close to 90°, and the plane of propagation of the aspect-angle scattered waves is almost perpendicular to the plane of the magnetic meridian. The oblique backscatter sounding signal is scattered near the uppermost point of the trajectories, i. e., backscattering takes place.

The ionospheric electron-density profile retrieved from the vertical sounding ionogram of the Cyclone-GPS ionosonde and considered invariable over the entire signal propagation path was used for the calculations. The basis for this is collation of this ionogram with that obtained at the Sura facility during heating, the time of their taking being different by no more than 1–2 min. The traces of the ionogram at the Sura facility during heating are highly suppressed in the O mode in the region of the heating frequency and critical frequencies f_{OF_2} due to a strong anomalous attenuation of the sounding signals [19]. But in the region where the traces of ionograms (X mode and part of the O mode) are clearly visible and acceptable for collation, the ionograms are almost identical: the frequencies and effective reflection altitudes coincide to a high accuracy with those on the ionograms taken above Kazan. This permitted us to neglect the impact of the horizontal gradients of the electron density in the ray-tracing calculations and consider its profile invariable. This approach can be applied when the ionosphere state is identical at both ends of the path: only in this case can the assumption about invariance of the profile along the path be considered justified. This assumption can be violated, e. g., by the appearance of traveling ionospheric disturbances, as well as by the passage through the solar terminator. In this case, it is necessary to allow for the impact of the horizontal electron-density gradients on the refraction of sounding and scattered signals.

For a detailed analysis and collation of the experimental data on September 24, 2010 with the calculations, we chose an ionogram recorded at 19:01 MSK (upper left panels in Figs. 1*a* and 3*a*), which shows traces (ionogram) of vertical sounding (marked in blue for the O- and X-mode components) and traces of aspect-scattered signals (oblique backscatter sounding ionogram), also corresponding to the O- and X-mode components (marked in red). The electron-density profile obtained by processing of the vertical sounding ionogram using the algorithm proposed in [20] was employed for the ray-tracing calculations. The dependence of the true reflection altitude on the frequency above the ionosonde, $h(f)$, is shown in Fig. 3*a*. The reflection altitude of the pump wave was $h_0 = 233$ km, the altitude of the maximum of the F_2 layer was equal to $h_{F_2} = 261$ km ($f_{OF_2} = 5.3$ MHz). Also, Fig. 3*a* shows the calculated curves (solid curves with markers) of delays of an aspect-scattered signal as functions of the sounding frequency, which coincide quite well with

TABLE 1.

f, MHz	h_r km,	n	$l_\perp$, m	τ, ms	R_{EW}, km	γ, degrees	X, km	Y, km
O-mode								
2.250	168.2	0.539	123.5	1.00	17.7	91.1	−0.6	−0.2
2.500	174.5	0.560	107.1	0.99	18.3	89.3	2.8	−0.2
2.750	180.8	0.559	97.6	0.98	19.0	87.9	0.2	3.5
3.000	186.1	0.561	89.1	0.98	19.6	89.5	−0.9	3.5
3.250	191.3	0.555	83.1	0.98	20.1	90.2	−2.5	4.3
3.500	195.8	0.559	76.7	0.99	20.6	91.7	−0.8	4.5
3.750	200.3	0.552	72.4	1.01	21.1	89.8	−0.2	4.7
4.000	204.4	0.552	67.9	1.02	21.5	89.5	1.9	4.6
4.250	208.6	0.545	64.7	1.03	21.9	89.4	1.4	4.8
4.500	213.2	0.535	62.3	1.05	22.4	89.7	1.1	4.9
4.750	218.0	0.520	60.6	1.07	22.9	89.3	0.6	4.9
5.000	223.1	0.511	58.7	1.10	23.5	89.8	0.1	4.8
5.250	229.0	0.494	57.8	1.13	24.1	90.2	−0.3	4.6
5.500	236.3	0.473	57.6	1.19	24.8	89.8	1.1	3.8
5.750	244.5	0.466	55.9	1.29	25.7	90.6	13.2	1.4
X-mode								
3.500	183.0	0.608	70.4	1.04	19.2	90.6	0.5	11.9
3.750	188.3	0.608	65.7	1.04	19.8	91.5	2.5	11.2
4.000	193.6	0.600	62.4	1.04	20.4	89.2	2.6	10.9
4.250	198.6	0.590	59.7	1.05	20.9	88.7	1.9	10.8
4.500	203.3	0.583	57.1	1.05	21.4	89.8	1.7	10.7
4.750	207.8	0.572	55.2	1.05	21.8	89.6	−0.8	10.9
5.000	212.4	0.562	53.3	1.07	22.3	88.7	−0.9	9.9
5.250	217.0	0.550	51.9	1.09	22.8	89.2	−0.1	10.7
5.500	222.2	0.541	50.4	1.11	23.4	88.4	−1.6	10.0
5.750	227.6	0.529	49.3	1.13	23.9	89.8	−2.1	11.1
6.000	233.6	0.522	47.9	1.17	24.5	90.1	1.0	10.8
6.125	238.1	0.505	48.5	1.20	25.0	90.3	−2.0	10.3
6.250	244.3	0.480	50.0	1.26	25.7	89.1	−4.6	12.1
6.350	250.0	0.465	50.8	1.32	26.3	89.7	−4.0	12.4
6.400	254.9	0.449	52.1	1.38	26.8	90.1	−3.6	12.8

the experimental oblique backscatter sounding ionograms.

The dependence of the transverse (to the geomagnetic field) scale of the scattering irregularity, calculated by the formula $l_\perp = c/(2fn)$, where c is the speed of light, f is the sounding frequency, and n is the refractive index of the radio wave at the scattering altitude, on the frequency f is shown in Fig. 3*b*. It is seen that the scales of scattering irregularities lie within the range $l_\perp \approx$ 48–124 m and decrease with increasing frequency.

The results of calculations of the parameters of the scattered signal (time delay τ, the altitude h_r of the scattering point, the angle γ at this point, and the coordinates X and Y of projection of the scattering point on the Earth's surface), the ionospheric parameters (refractive index n, the scale $l_\perp$ of the scattering irregularity), and the half-beamwidth of the Sura antenna at the scattering altitude for the case of vertical heating along the east–west line, R_{EW} ($R_{NS} \sim 1.5R_{EW}$) and both scattering modes are summarized in Table 1.

Note that Table 1 and Fig. 3*a* show (at each frequency f) the τ values determined as the average

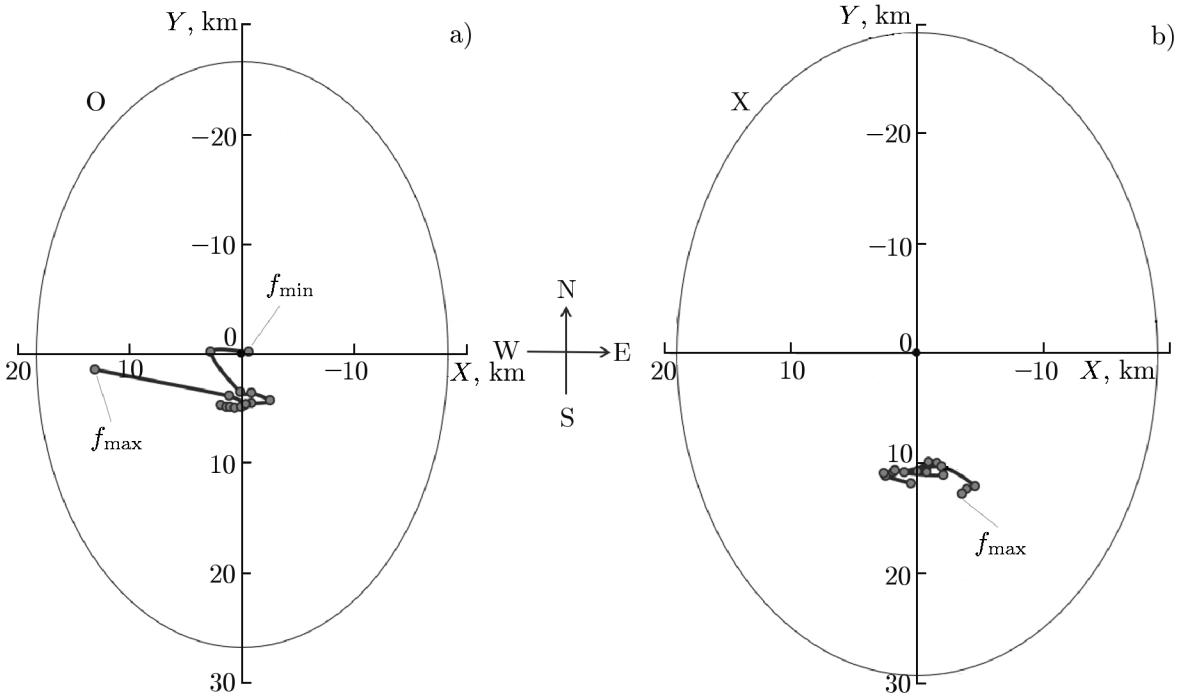

Fig. 4. Projections of the signal scattering points on the Earth's surface in the frequency range $f_{\min} < f < f_{\max}$ for the O mode (a) and X mode (b) under vertical heating. The ellipse corresponds to the heating volume (it has a radius equal to the half-beamwidth of the Sura facility at the scattering altitude of the O-mode signal with a frequency of 2.25 MHz and the X-mode signal with a frequency of 3.5 MHz). Panel a: $f_{\min} = 2.25$ MHz and $f_{\max} = 5.75$ MHz. Panel b: $f_{\max} = 6.4$ MHz.

of the values obtained for the entire set of incidence angles for which the scattered signal comes into the reception zone. All the parameters are given in Table 1 and in Figs. 3b, 4, and 5 for the same average values of τ. In this case, the accuracy of determination of τ is governed, as was indicated above, by the thickness of the ionogram trace $\Delta\tau \approx \Delta H/c \approx 50$–$100$ μs. In fact, we should speak not of a "scattering point," but of a region of finite dimensions responsible for scattering at each frequency f. The size of this region can be estimated from the following considerations. First, the scattered signal is formed in a region of the order of several wavelengths $\lambda = c/(nf)$ along the direction of propagation of the incident wave and of the order of several Fresnel zones $r \approx (\lambda H)^{1/2}$ across this direction. Thus, the transverse scale of the region in the frequency range in which scattered signals are observed varies from 3 to 6 km. Secondly, the finite width of the trace (the spread $\Delta\tau$) may indicate that not only the backscatter signal is observed. In particular, the analysis of the experimental data performed in [13] showed that when the cone of incident signals has an opening of about 1°, signals with angles of $85° < \gamma < 95°$ in the scattering region, i. e., $\pm 5°$ from the direction across the magnetic field $\mathbf{B}$, can arrive at the receiving antenna. Finally, the region occupied by irregularities is quite extended and can fill almost the entire radiation pattern of the heater and even go beyond its boundaries. In this case, scattering can occur at different angles of incidence of the sounding waves on the ionosphere, some of them will be detected by the ionosonde, which will give an increase in $\Delta\tau$ and, accordingly, an increase in the size of the region responsible for scattering. These issues are discussed in more detail in [13]. In this paper, we are speaking about the "scattering point," meaning the center of the scattering region.

Figures 4 and 5 show the results of the analysis of ray-tracing calculations for sounding signals, which correspond to those given in Table 1. Figure 4 shows projections of the signal scattering points on the Earth's surface for the O mode (a) and X mode (b).

Figure 5 shows projections of the signal scattering points on mutually perpendicular north–south and east–west planes in the studied frequency range for the O mode (a) and X mode (b). The dashed line shows

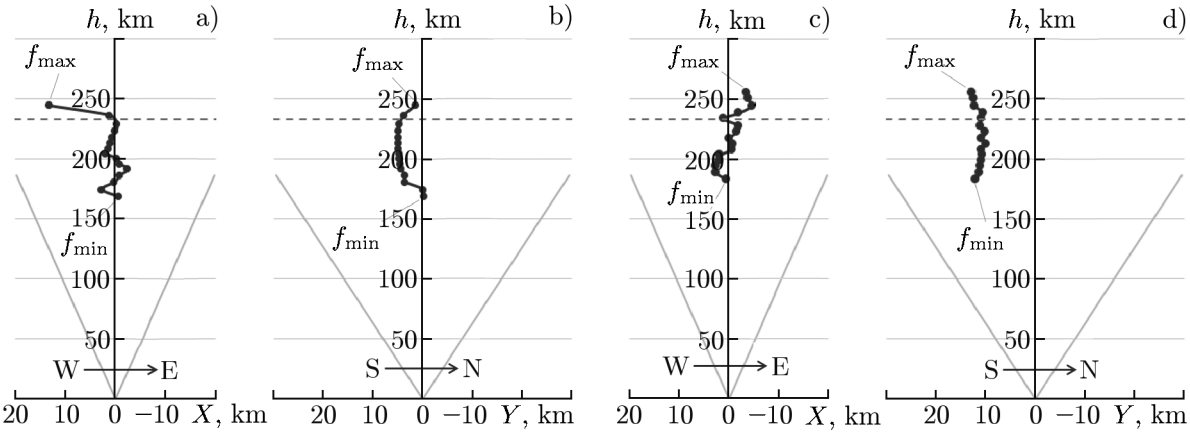

Fig. 5. Projections of the signal scattering points on mutually perpendicular north–south and east–west planes in the frequency range $f_{min} < f < f_{max}$ for the O and X modes. The dashed line shows the altitude corresponding to the reflection level of the pump wave at a frequency of 4.74 MHz. Panels *a* and *b*: $f_{min} = 2.25$ MHz and $f_{max} = 5.75$ MHz. Panels *c* and *d*: $f_{min} = 3.5$ MHz and $f_{max} = 6.4$ MHz.

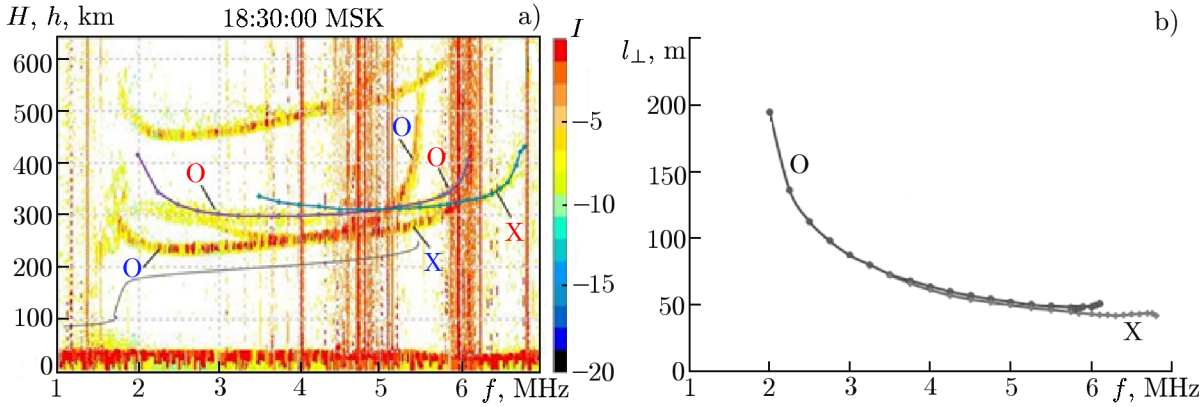

Fig. 6. Panel *a*: ionograms of vertical (marked in blue) and oblique backscatter (marked in red) sounding with oblique heating of the ionosphere (September 20, 2010, Cyclone-GPS ionosonde), calculated curves of the delay time of the scattered signal in units of the effective altitude H (solid curves with markers), and the dependence of the true reflection altitudes h on the frequency according to vertical sounding data (solid curve). Panel *b*: dependence of the transverse scale $l_\perp$ of the scattering irregularity on the sounding frequency.

the altitude $h_0 = 233$ km corresponding to the level of reflection of the pump wave at a frequency of 4.74 MHz. A shift of the scattering region to the west at high frequencies near 5.75 MHz is seen in the diagrams for the O mode. In the main (average) frequency range of aspect-angle scattering, the scattering region is quite narrow and does not go beyond the Sura radiation pattern. While in the main frequency range the O mode of the aspect-angle scattering falls into the center of exposure of the radiation pattern, the X-mode scattering region is localized in the southern part of the radiation pattern (is shifted by 10–15 km southward). The scattering altitude decreases by 72–77 km with a decrease in the sounding frequency, covering the altitude ranges both above and below the reflection level of the pump wave.

4. CALCULATION RESULTS FOR OBLIQUE HEATING

The analysis of experimental data was similar for oblique heating of the ionosphere on September 20, 2010. An ionogram recorded at 18:30 MSK was chosen, the reflection altitude of the pump wave was $h_0 = 222$ km, and the altitude of the maximum of the F_2 layer was $h_{F_2} = 252$ km ($f_{OF_2} = 5.5$ MHz). Figure 6*a* shows the calculated delay curves of the aspect-angle scattered signals of the O and X modes

TABLE 2.

f, MHz	h_r, km	n	$l_\perp$, km	τ, ms	R, km	γ, degrees	X, km	Y, km	X_c, km	Y_c, km	$X - X_c$, km	$Y - Y_c$, km
O mode												
2	180.8	0.385	194.7	1.39	19.0	89.8	14.4	26.3	7.3	37.7	7.1	−11.4
2.25	184.9	0.489	136.2	1.15	19.4	89.9	14.6	44.7	7.5	38.6	7.1	6.1
2.50	188.9	0.534	112.4	1.07	19.8	88.9	12.8	49.4	7.6	39.4	5.2	10.0
2.75	192.2	0.557	97.9	1.03	20.2	89.9	10.6	52.1	7.8	40.1	2.8	12.0
3.00	194.8	0.574	87.1	1.01	20.5	90.7	10.9	53.8	7.9	40.7	3.0	13.2
3.25	197.3	0.576	80.0	1.00	20.7	90.1	7.8	51.2	8.0	41.2	−0.2	10.0
3.50	199.4	0.587	72.9	1.00	21.0	89.0	10.9	50.7	8.1	41.6	2.9	9.1
3.75	201.7	0.587	68.1	1.00	21.2	89.4	9.7	51.0	8.2	42.1	1.5	8.9
4.00	203.8	0.586	63.9	1.00	21.4	90.2	9.18	51.3	8.3	42.5	0.9	8.7
4.25	205.9	0.589	59.9	1.01	21.6	89.5	11.0	51.8	8.3	43.0	2.7	8.8
4.50	208.1	0.586	56.9	1.01	21.9	90.8	10.6	51.9	8.4	43.4	2.2	8.4
4.75	210.6	0.580	54.4	1.03	22.1	88.9	10.9	52.0	8.5	43.9	2.4	8.0
5.00	213.4	0.572	52.4	1.04	22.4	90.0	10.7	52.0	8.6	44.5	2.1	7.4
5.25	216.2	0.570	50.1	1.07	22.7	88.9	13.7	53.3	8.7	45.1	5.0	8.2
5.50	219.9	0.555	49.1	1.08	23.1	89.9	12.4	52.0	8.9	45.9	3.5	6.1
5.75	224.1	0.544	47.9	1.12	23.6	90.1	15.1	52.1	9.1	46.8	6.1	5.3
5.80	224.9	0.544	47.5	1.14	23.6	89.9	17.0	54.0	9.1	46.9	7.9	7.0
5.85	225.9	0.541	47.3	1.15	23.7	89.8	17.9	54.0	9.1	47.1	8.8	6.9
5.90	228.2	0.524	48.4	1.17	24.0	89.7	15.1	53.3	9.2	47.6	5.8	5.7
6.00	231.3	0.513	48.7	1.22	24.3	89.2	19.4	52.8	9.4	48.3	10.1	4.6
6.05	234.3	0.498	49.8	1.27	24.6	90.0	21.2	54.3	9.5	48.9	11.7	5.4
6.10	237.8	0.484	50.8	1.35	25.0	90.0	28.5	51.8	9.6	49.6	18.9	2.2
X mode												
3.50	193.7	0.594	72.1	1.13	20.4	90.6	6.6	59.6	7.8	40.4	−1.2	19.2
3.75	196.4	0.604	66.1	1.09	20.6	90.0	8.7	60.0	7.9	41.0	0.8	19.0
4.00	198.7	0.613	61.1	1.07	20.9	89.0	12.1	58.9	8.0	41.5	4.1	17.4
4.25	201.0	0.617	57.2	1.06	21.1	90.2	13.8	59.6	8.1	42.0	5.7	17.7
4.50	203.5	0.669	49.8	1.05	21.4	91.6	9.3	57.8	8.2	42.5	1.1	15.3
4.75	205.7	0.607	52.0	1.05	21.6	90.6	10.3	59.3	8.3	43.0	1.9	16.4
5.00	208.1	0.604	49.7	1.05	21.9	89.8	9.7	59.1	8.4	43.4	1.3	15.7
5.25	210.6	0.599	47.7	1.05	22.1	90.5	9.4	59.0	8.5	44.0	0.9	15.1
O mode												
5.50	213.6	0.587	46.4	1.06	22.5	90.8	6.9	60.2	8.6	44.6	−1.7	15.7
5.75	216.6	0.582	44.8	1.07	22.8	90.7	7.9	60.4	8.8	45.2	−0.8	15.2
5.85	217.8	0.582	44.0	1.08	22.9	90.9	9.2	60.6	8.8	45.5	0.4	15.2
6.00	219.8	0.579	43.1	1.09	23.1	90.8	10.6	60.9	8.9	45.9	1.7	15.0
6.10	221.4	0.576	42.7	1.10	23.3	89.8	11.3	60.0	9.0	46.2	2.6	13.8
6.20	223.3	0.568	42.5	1.11	23.5	90.4	10.1	59.9	9.03	46.6	1.1	13.3
6.30	225.0	0.565	42.1	1.12	23.7	90.8	11.0	61.1	9.1	47.0	1.94	14.2
6.40	227.8	0.552	42.5	1.14	23.9	90.4	8.7	60.9	9.2	47.5	−0.5	13.4
6.50	231.1	0.538	42.9	1.17	24.3	89.9	7.7	61.0	9.4	48.2	−1.6	12.8
6.60	235.3	0.523	43.4	1.22	24.7	90.2	8.3	61.4	9.5	49.1	−1.2	12.3
6.70	241.3	0.509	44.0	1.32	25.4	89.9	15.1	63.1	9.8	50.4	5.3	12.7
6.75	244.1	0.511	43.4	1.41	25.7	90.5	26.6	65.2	9.9	50.9	16.7	14.3
6.80	244.0	0.526	41.9	1.44	25.6	89.6	38.0	64.4	9.9	50.9	28.1	13.5

and the dependence of the true reflection altitude on the sounding frequency. The dependence of the scale of the scattering irregularities on the sounding-signal frequency is shown in Fig. 6*b*. As in the case of vertical heating, the transverse scale of the scattering irregularities, $l_\perp \approx 42$–195 m, decreases with increasing

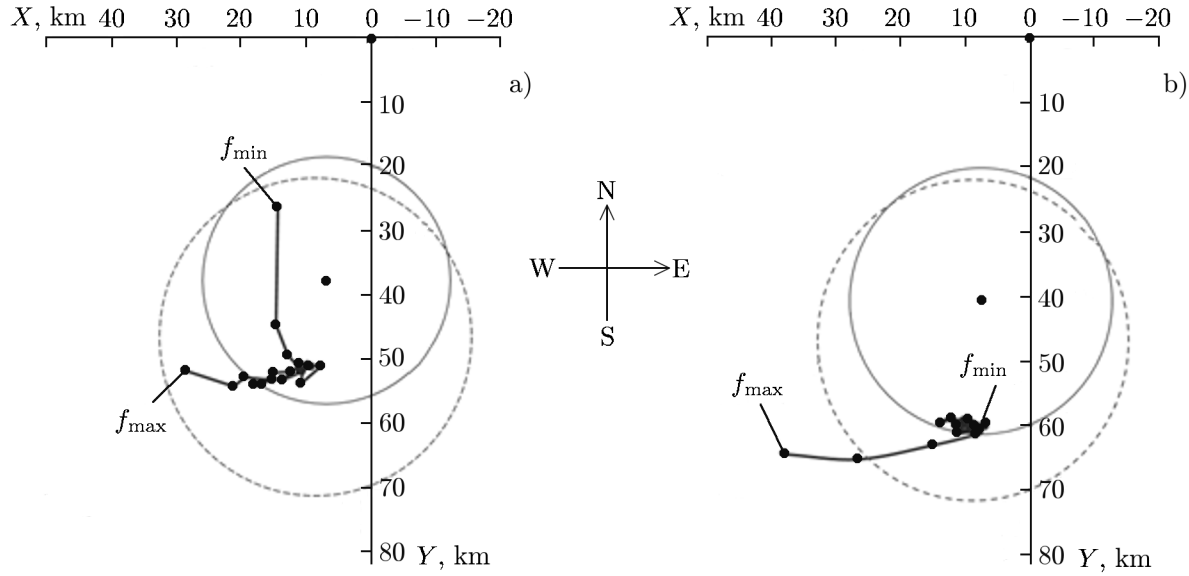

Fig. 7. Projections of the signal scattering points on the Earth's surface in the frequency range $f_{min} < f < f_{max}$ for the O and X modes under vertical heating. The dashed line shows the circle corresponding to the maximum possible transverse size of the radiation pattern at the altitude of reflection of the pump wave ($f_0 = 4.74$ MHz). Panel *a*: $f_{min} = 2$ MHz and $f_{max} = 6.1$ MHz. Panel *b*: $f_{min} = 3.5$ MHz and $f_{max} = 6.8$ MHz.

frequency. The results of calculations of the parameters of the scattered signal and the ionosphere, as well as the corresponding characteristics of the Sura facility for the case of oblique heating and both scattering modes are summarized in Table 2 (here, X_c and Y_c are the coordinates of the projection center of the Sura radiation pattern).

Figure 7 shows the projections of the signal scattering points on the Earth's surface in the frequency range $f_{min} < f < f_{max}$ for the O and X modes. The circle corresponds to the heating volume and has a radius equal to half-width of the Sura radiation pattern, which is tilted by 12° southward at the scattering altitude of the O-mode signal with a frequency of 2 MHz and the X-mode signal with a frequency of 3.5 MHz. The Sura facility is located at the point with coordinates (0; 0), i. e., in the north, and the sounding signal comes from the east. Figure 8 shows the projections of the signal scattering points on mutually perpendicular north–south and east–west planes in the studied frequency range for the O mode (*a*) and X mode (*b*). The dashed line shows the altitude $h_0 = 222$ km corresponding to the level of reflection of the pump wave at a frequency of 4.74 MHz.

Figures 7 and 8 show that the shift effect is more pronounced for the case of oblique heating than for the vertical one, since there is a notably greater shift of the scattering region to the west for both modes at high frequencies, a shift to the north for the O mode at low frequencies, and a common shift to the south in the main part of the frequency range. However, the scattering region almost does not go beyond the boundaries of the Sura radiation pattern, although it is located mainly closer to its southern boundary. The altitude range of the scattering region at different frequencies is 54–57 km.

5. CONCLUSIONS

Using the analysis of the ionograms recorded during the continuous operation of the Sura facility by the Cyclone-GPS ionosonde located 172 km east of it (Kazan — Vasilsursk — Kazan path), it is shown that the ionogram traces corresponding to the O- and X-mode components of the aspect-angle scattered waves can be employed to study the properties of the small-scale field-aligned electron-density irregularities occurring due to the heater radiation. The analysis was conducted on the basis of the ray-tracing calculations for the oblique backscatter sounding signals in the frequency range 2–7 MHz, assuming that the electron-density profile is invariable along the signal propagation path. This assumption is justified by the identity

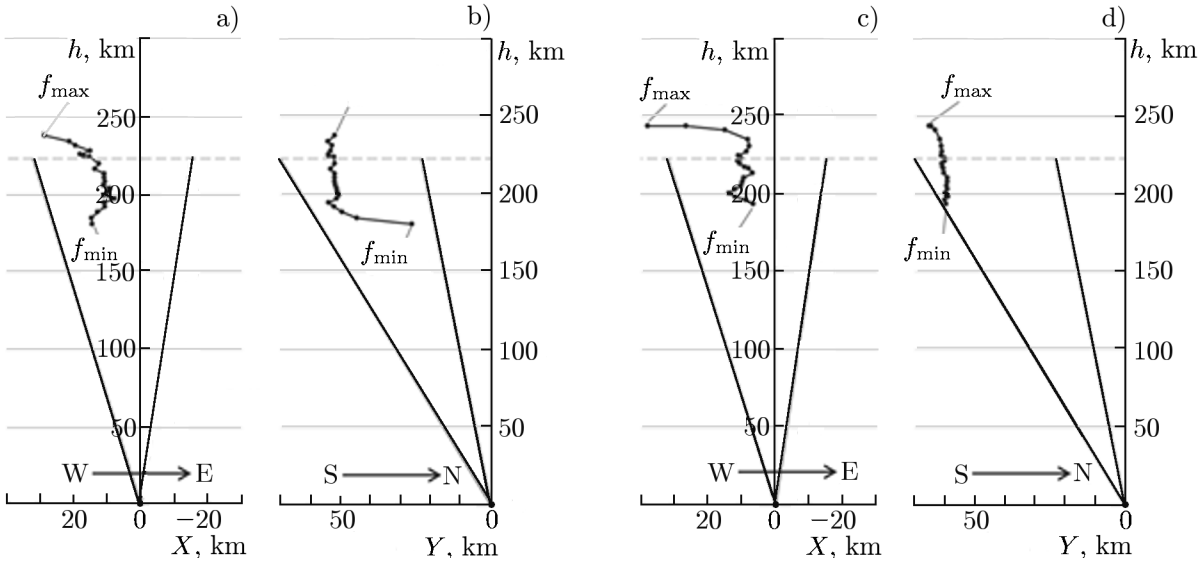

Fig. 8. Projections of the signal scattering points on mutually perpendicular north–south and east–west planes in the frequency range $f_{min} < f < f_{max}$ for the O and X modes. The dashed line shows the altitude corresponding to the reflection level of the pump wave at a frequency of 4.74 MHz. Panels *a* and *b*: $f_{min} = 2$ MHz and $f_{max} = 6.1$ MHz. Panels *c* and *d*: $f_{min} = 3.5$ MHz and $f_{max} = 6.8$ MHz.

of the ionograms recorded simultaneously at the Sura facility and the Cyclone-GPS ionosonde in the facility radiation pause and the relatively small length of the path. The advantage of ionograms in comparison with the data of the same ionosonde when it operates at several fixed frequencies (see [13, 14]) is the possibility of using an almost continuous spectrum of oblique backscatter sounding signals. In this paper, the calculations were performed with a frequency step of 250 kHz, which is half the separation of fixed frequencies in [13, 14], while there is a possibility for analysis with a step of 20–25 kHz. In fact, we analyze the continuous dependence of the studied parameters (the position of the center of the scattering region and the scale of the scattering irregularities) on the frequency of the oblique backscatter sounding signal over the entire range where the corresponding ionogram is observed. Thus, the development of the method and the novelty of the studies consist in the increased frequency (and, consequently, spatial) resolution when the position of the artificial decametric ionospheric irregularities responsible for the aspect-angle scattering of radio waves on a short path is determined from oblique backscatter sounding ionograms. As a result of a joint analysis of the experimental data and the ray-tracing calculations, we have found the following.

The minimum frequency of the observed scattered signals does not fall below the critical frequency of the *E* layer (according to the sensitivity threshold of the receiving equipment of the Cyclone-GPS ionosonde), approaching it in the evening measurements. The MOF of scattering for both radiation modes can exceed the critical frequencies.

During the transition from daytime to evening measurements between 17:30 and 19:00 MSK on September 20, 2010, the dynamics of the scattered signal was observed depending on the time of the day. Namely, there was a decrease in the least observed scattering frequency from 3.5 MHz to 2.0 MHz and an extension of the high-altitude scattering interval, which confirms the results of the previous studies [13, 14].

In the main frequency range, the scattering is localized in a narrow region that does not go beyond the radiation pattern of the Sura facility, both in the case of vertical and oblique heating. While in the main frequency range the O mode of aspect-angle scattering falls into the center of exposure of the radiation pattern, the X-mode scattering region is localized in the southern part of the radiation pattern (shifted by 10–15 km southward).

The scattering region is shifted at the extreme points of the frequency range for the aspect-angle scattering. For the O mode, vertical heating, and upper limit (5.75 Hz), the shift is to the west (13 km), for

the O mode, oblique heating, and lower limit (2 MHz), the shift is to the north (24 km), for the O mode, oblique heating, and high frequencies (6.1 MHz), the shift is to the west (19 km), and for the X mode, oblique heating, and upper limit (6.8 MHz), the shift is to the west (28 km). The shift effects are more pronounced for oblique heating.

Scattering occurs both above and below the reflection level of the pump wave ($h_0 = 233$ km with vertical heating and $h_0 = 222$ km with oblique heating), the scattering altitude does not exceed the altitude of the F_2-layer maximum. It is equal to $h_{F_2} = 261$ km ($f_{OF_2} = 5.3$ MHz) with vertical heating and $h_{F_2} = 252$ km ($f_{OF_2} = 5.5$ MHz) with oblique heating. The altitude of the scattering region decreases by 52–77 km with a decrease in the sounding frequency.

The scale of scattering irregularities transverse to the geomagnetic field lies in the range of values $l_\perp \approx 42$–195 m and increases with a decrease in the sounding frequency. If we assume that the region of generation of these irregularities lies near the reflection level of the pump wave reflection, then, according to observations, for scattering signals at the edges of the sounding frequency range (2 and 7 MHz), the vertical size of the field-aligned scattering irregularities reaches 22 km and 65 km above and below the center of the heated volume, respectively (see Figs. 5 and 8 and Tables 1 and 2).

The measurement of the characteristics of scattered signals in the range 2–7 MHz and the calculation of their traces on short paths make it possible to analyze the structure of the heated ionospheric volume in the range of transverse scales of artificial irregularities $l_\perp \approx 40$–200 m. The results of similar studies on long paths in the frequency range 7–30 MHz, including the chirp signal sounding, performed simultaneously in the experiments on September 20–24, 2010, are given in [21–23]. A collation of all the data enables one to study the spatial distribution of irregularities in a wider range of scales $l_\perp \approx 10$–200 m.

The paper was supported by the Russian Science Foundation (project No. 20-12-00197, conclusions based on the results of measurements and calculations), the Russian Foundation for Basic Research (project No. 18-02-00622, ray-tracing calculation, project No. 19-02-00343, analysis of the experimental data). The experiments were performed using the Sura large-scale research facility. At present, this facility is supported by a grant from the Ministry of Science and Higher Education of the Russian Federation, received within the framework of the Federal Target Program "Research and development in priority areas of development of the scientific and technological complex of Russia for 2014–2020," the unique project identifier RFMEFI62020X0003, agreement No. 075–15–2020–529.

REFERENCES

1. P. A. Fialer, *Radio Sci.*, **9**, No. 11, 923–940 (1974). https://doi.org/10.1029/RS009i011p00923
2. G. H. Barry, *Radio Sci.*, **9**, No. 11, 1025–1032 (1974). https://doi.org/10.1029/RS009i011p01025
3. P. B. Rao and G. D. Thome, *Radio Sci.*, **9**, No. 11, 987–996 (1974). https://doi.org/10.1029/RS009i011p00987
4. L. M. Erukhimov, S. A. Metelev, N. A. Mityakov, et al., *Radiophys. Quantum Electron.*, **30**, No. 2, 156–171 (1987). https://doi.org/10.1007/BF01034489
5. V. L. Frolov, L. M. Erukhimov, S. A. Metelev, and E. N. Sergeev, *J. Atm. Solar-Terr. Phys.*, **59**, No. 12, 2317–2333 (1998). https://doi.org/10.1016/S1364-6826(96)00126-5
6. A. M. Nasyrov, *Scattering of Radio Waves by Anisotropic Ionospheric Irregularities* [in Russian], Kazan Federal University, Kazan (1991).
7. V. P. Uryadov, N. V. Ryabova, V. A. Ivanov, and V. V. Shumaev, *J. Atm. Terr. Phys.*, **57**, No. 11, 1263 (1995). https://doi.org/10.1016/0021-9169(94)00115-5
8. V. P. Uryadov, G. G. Vertogradov, V. G. Vertogradov, et al., *Radiophys. Quantum Electron.*, **50**, No. 8, 611–618 (2007). https://doi.org/10.1007/s11141-007-0053-5

9. V. P. Uryadov, G. G. Vertogradov, A. A. Ponyatov, et al., *Radiophys. Quantum Electron.*, **51**, No. 12, 910–922 (2008). https://doi.org/10.1007/s11141-009-9095-1
10. V. P. Uryadov, G. G. Vertogradov, V. G. Vertogradov, et al., *Radiophys. Quantum Electron.*, **52**, No. 4, 241–251 (2009). https://doi.org/10.1007/s11141-009-9136-9267–278
11. N. V. Bakhmet'eva, Y. A. Ignat'ev, S. A. Dmitriev, and P. B. Shavin, *Geomagn. Aéron.*, **32**, No. 3, 180–185 (1992).
12. A. Herberg, H. Deblom, B. Thide, et al., *Radio Sci.*, **18**, No. 6, 840–850 (1983). https://doi.org/10.1029/RS018i006p00840
13. N. A. Pogorelko, E. N. Sergeev, S. M. Grach, et al., *Radiophys. Quantum Electron.*, **61**, No. 2, 83–97 (2018). https://doi.org/10.1007/s11141-018-9873-8
14. E. N. Sergeev, E. Y. Zykov, A. D. Akchurin, et al., *Radiophys. Quantum Electron.*, **55**, Nos. 1–2, 71–84 (2012). https://doi.org/10.1007/s11141-012-9350-8
15. S. M. Grach, N. A. Pogorelko, and V. A. Yashnov, *Vestn. Nizhegor. Univ. Lobach.*, No. 6–1, 43–50 (2012).
16. http://wdc.kugi.kyoto-u.ac.jp/igrf/
17. Y. A. Kravtsov and Y. I. Orlov, *Geometric Optics of Inhomogeneous Media* [in Russian], Nauka, Moscow (1980).
18. E. L. Cherenkova and O. V. Chernyshev, *Propagation of Radio Waves*, [in Russian], Radio i Svyaz', Moscow (1984).
19. G. G. Getmantsev, G. P. Komrakov, Y. S. Korobkov, et al., *JETP Lett.*, **18**, No. 10, 364–366 (1973).
20. T. L. Gulyaeva, *Fortran Program ITERAN for Iterative $N(h)$ Analysis of Ionograms* [in Russian], VINITI, Moscow (1979).
21. G. G. Vertogradov, E. G. Vertogradova, V. P. Uryadov, et al., *Radiophys. Quantum Electron.*, **55**, Nos. 1–2, 1–12 (2012). https://doi.org/10.1007/S11141-012-9345-5
22. G. G. Vertogradov, V. P. Uryadov, V. G. Vertogradov, et al., *Radiophys. Quantum Electron.*, **58**, No. 5, 307–317 (2015). https://doi.org/10.1007/s11141-015-9605-2
23. G. G. Vertogradov, V. P. Uryadov, V. G. Vertogradov, et al., *Radiophys. Quantum Electron.*, **58**, No. 6, 381–389 (2015). https://doi.org/10.1007/s11141-015-9613-2